Sayed, Ahmad M.; Abouelatta, Mohamed A.; Badawi, Mohamed; Mahmoud, Karar; Lehtonen, Matti; Darwish, Mohamed M. F.

Novel accurate modeling of dust loaded wire-duct precipitators using FDM-FMG method on one fine computational domains

Published in:
Electric Power Systems Research

DOI:
10.1016/j.epsr.2021.107634

Published: 01/02/2022

Document Version
Publisher's PDF, also known as Version of record

Electric Power Systems Research 203 (2022) 107634

Contents lists available at ScienceDirect

Electric Power Systems Research

journal homepage: www.elsevier.com/locate/epsr

Novel accurate modeling of dust loaded wire-duct precipitators using FDM-FMG method on one fine computational domains

Ahmad M. Sayed [a], Mohamed A. Abouelatta [a], Mohamed Badawi [a], Karar Mahmoud [b,c], Matti Lehtonen [b], Mohamed M.F. Darwish [a,b,*]

[a] Department of Electrical Engineering, Faculty of Engineering at Shoubra, Benha University, 11629 Cairo, Egypt
[b] Department of Electrical Engineering and Automation, School of Electrical Engineering, Aalto University, FI-00076 Espoo, Finland
[c] Department of Electrical Engineering, Faculty of Engineering, Aswan University, 81542 Aswan, Egypt

ARTICLE INFO

Keywords:
Electrostatic precipitators
Full multigrid method
Fine computational domain
Finite difference method
Ion mobility

ABSTRACT

Worldwide, electrostatic precipitators (ESP) have been extensively utilized to separate fine particles for diverse large-scale industrial applications. In this regard, this paper presents a novel approach for modeling the dust-loaded ESP on the fine computational domain where the need for a fast solver arises. Unlike the previously published numerical techniques, the finite difference method (FDM) integrated with a full multi-grid method (FMG), labeled FDM-FMG, is developed to resolve Poisson and continuity equations on one fine computational domain. For clean and dust-loaded ESP, the proposed FMG is checked versus successive over-relaxation (SOR) on fine domains where the proposed one is greatly transcendent in terms of convergence characteristics and hence the computational performance (CPU time). For the first time, two major issues are highlighted and solved: the first concerning issue is the chosen ion mobility as an important factor in the simulation results and the second one is choosing an optimal computational grid for dust loaded precipitators that grantees both low truncation and roundoff errors, results in well-matched with experimental measurements nominated in the previous publishing. The novel idea of working on various grid sizes and tracking the optimal ones gives the FDM-FMG an advantage of predicting a precise picture for the electrical situations in industrial ESP over the other numerical techniques. After all, the impact of changing the spacing between the different wires and the height of the ionized wires on the distributions of current, ion, and particle charge densities on the ground are deeply simulated and presented in dust-loaded ESP. The proposed FDM-FMG can be a promising tool for the designers and manufacturers of precipitators, thanks to its superior computational performance.

1. Introduction

Recently, the world witnessed a growth in electrical power generation which is met by an increase in the gas flows resulted from the industrial power stations. These industrial power plants cause air pollution which can be minimized by using electrostatic precipitators [1, 2]. Besides, precipitators remove the sulphuric acid produced from gold recovery technologies [3, 4]. The most widespread type of precipitator is the wire-duct electrostatic precipitator (ESP) consisting of a number of paths formed by parallel grounded plates with several wires centrally located between the grounded plates. A detailed explanation of the basic operation of wire-duct ESPs is illustrated in [5]. Several numerical methods are established to study the electrical properties including the voltage and current characteristics in clean air electrostatic precipitators. Accordingly, the electrical problems concerning the operation during different loading conditions can be predicted. The most affecting parameters on the performance of wire-duct ESPs are wire diameter, the distance between wires as well as the height of the wire over the grounded plate. The numerical techniques implemented to model the corona problem in ESPs are classified as follows: finite difference method (FDM) [2, 6, 7], finite element method (FEM) integrated with FDM [8], boundary element method (BEM) combined with the method of characteristics (MOC) [9], BEM integrated with FDM [10], FEM [11], charge simulation method (CSM) [12], and FEM combined with MOC [13–15]. Cristina and Feliziani [16] use the FEM to model the dust-loaded precipitator for calculating the V-I curves and precipitation efficiencies for different sizes of particles.

In the literature, there are several numerical based methods for ESPs.

* Corresponding author.
E-mail addresses: mohamed.m.darwish@aalto.fi, mohamed.darwish@feng.bu.edu.eg (M.M.F. Darwish).

https://doi.org/10.1016/j.epsr.2021.107634
Received 13 April 2021; Received in revised form 8 October 2021; Accepted 13 October 2021
Available online 25 October 2021

Castle [17] formulated an approximate analytical expression for the simulation of a dust-loaded precipitator. Besides, Abdel-Sattar [18] implements the CSM to model the cement and steel particles. Al Hamouz et al. [19] uses a finite element-based method integrated with an adapted MOC to calculate the current density shapes, corona power losses, and corona current in wire-duct ESP under particle loading conditions. On the other side, a group of experimental work has been conducted below dust loading circumstances. For instance, Jedrusik et al. [20] studied the effect of changing the physicochemical features of the fly ash on collection proficiency. Miller et al. [21] examined the effect of diverse electrode designs on the efficiency of the wire-duct ESP. Zhuang et al. [22] perform experimental and theoretical research studies on the performance of a cylindrical precipitator for the gathering of ultra-fine particles ranges between (0.05–0.5 μm). Bacchiega et al. measured the mass collection rates along with a pilot wire-duct ESP in an industrial environment [23]. Modeling of the electrostatic field in the dust-loaded precipitators on fine computational domains can provide the manufactures and designers with valuable guidelines for improving the performance of precipitators and dust collection efficiency.

In general, all the numerical techniques are time-consuming when dealing with fine domains especially in solving the Poisson equation. The FDM is utilized to model the corona problematic wire-duct ESPs, by approximating Poisson and continuity equations by the difference equations. Among the conventional iterative procedures used to resolve the finite difference equations are: 1) Jacobi method, 2) Gauss-Seidel method, and 3) successive over-relaxation technique (SOR). These iterative techniques are inefficient and have poor convergence when the rectangular grid turns out to be finer and finer [2, 24]. Accordingly, on fine computational domains, these classical iterative techniques consume an extreme computational time to converge to a certain optimal value. So, the need for a fast convergent iterative solver arises. The full multigrid method (FMG) solves the above-mentioned problem by using many grids of dissimilar mesh sizes. In this method, the fine computational domain is transferred to a coarser domain, where one of the traditional iterative approaches can be applied to resolve the coarser grid. Later, by grid transfer operators, the solution is used as an upgraded primary guess for the finer grids [24, 25, 26, 27, 28]. Most of the preceding research studies are missing to accurately model the dust-loaded ESP on one fine computational domain by the combination of FDM and the FMG solver, which is covered in this work.

To cover the abovementioned gap in the literature, this study is aiming to propose the finite difference method combined with the full multigrid method (FDM-FMG) to be implemented for modeling the dust-loaded ESP on one fine computational domain. Firstly, FDM-FMG is used to model the clean air ESP and is validated with previous experimental work. The convergence characteristics of this technique were demonstrated to be better than the other classical iterative methods, so less computational time is needed. Secondly, the problem of choosing the ion mobility value is discussed for the first time. Finally, the FDM-FMG is used to track the optimal computational grid for dust-loaded precipitators that ensures both low truncation as well as round-off errors. This optimal grid is tested against other published numerical techniques for previous published experimental measurements and better agreement is reached. Using this optimal grid, the impact of changing the spacing between wires as well as the height of the ionized wires in dust-loaded precipitators on the distributions of current, ion, and particle densities on the ground are intensively investigated.

The novelty of this paper can be concluded as follows:

- The FDM has applied one very fine computational domain in dust-loaded precipitators for the first time taking into consideration both truncation and round-off errors.
- With the help of the FMG solver, FDM becomes time efficient on different tolerances.
- The proposed FDM-FMG gives a more confident value of the chosen ion mobility without the need for excessive experimental efforts to measure it.
- FDM-FMG is an excellent prediction tool for the electrical properties in both clean air and dust-loaded precipitators.
- It is applicable to choose the optimal computational grid for any commercial dust loaded precipitators that grantees both low truncation and roundoff errors and can be a prediction tool for the change of dissimilar design parameters on the electrical conditions of the precipitator, and this advantage reduces the effort for the precipitators' designers.

2. Methods of analysis

2.1. Boundary conditions and simplifying assumptions

Because of the symmetry of the issue, only one-quarter of the computational domain is taken into consideration, Fig. 1. The boundary conditions and simplifying assumptions are [2]:

1) The voltage on the wire equals the applied voltage;
2) The E_x value at A, B points, and along with BC, CD, and AD lines, equals zero;
3) The E_y value equals zero at A and B points, and along with line AB;
4) Along line CD, the potential is equal to zero;
5) The mobility of ions is constant;
6) Diffusion of ions is ignored;
7) At point A, $\rho = \rho_o$, and the charge density, ρ_o, is determined by [2].

$$\rho_o = \frac{2S_x j_p}{\pi k r f \left(30\delta + 9\sqrt{\frac{\delta}{r}}\right)} \times 10^{-3} \quad (1)$$

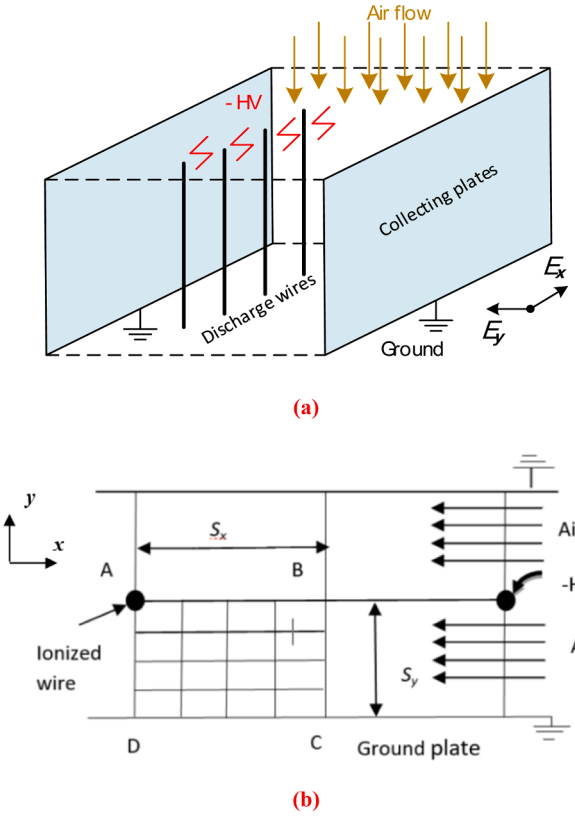

Fig. 1. Dust loaded wire-duct precipitator; (a) 3D view, and (b) 2D view for computational domain.

The air density factor is given by [2]:

$$\delta = \frac{293\,p}{760\,(t+273)} \tag{2}$$

in which f denotes the factor of surface roughness, δ denotes the air density factor, and r is the radius of the ionized wire (cm). j_p, S_x, t, and p are, respectively, the average current density on the plate (A/m^2), the half spacing between the ionized wires (m), the temperature in Celsius, and the pressure in mmHg.

The geometry under consideration is bounded geometry, as shown in fig (1) in the manuscript the domain between the two wires is divided into four symmetric co-domains. At point A the voltage at any node above A is the same at the corresponding nodes under A directly, so $E_y = 0$. Also, at any node on the right of A is the same potential as the corresponding nodes on the left of point A, so $E_x = 0$. The same discussion is applicable for point B.

2.2. Simulation of dust

The presence of the dust particles in electrostatic precipitators impacts the distribution of the electric field as well as current density. The total space charge density ρ_t can be defined by the following equation:

$$\rho_t = \rho + \rho_p \tag{3}$$

in which ρ_t represents the total space charge density (C/m^3), ρ represents the space charge density of ions, and ρ_p represents the space charge density of particles. So, the space charge density of dust particles is given by the following:

$$\rho_p = N_P \times q_s \tag{4}$$

where N_P and q_s represent the number of dust particles per unit volume and the saturation charge acquired by the field, respectively. So, the dust particle number per unit volume can be given by [19]:

$$N_P = \frac{3\,C_D}{4\,\pi\,g\,R_p^3} \tag{5}$$

where C_D is the concentration of dust particles (g/m^3), R_p is the radius of the particle, and g is the specific gravity (g/m^3). The saturation charge is given by [19]:

$$q_s = 4\pi\varepsilon_0\,R_p^2\frac{3\,\varepsilon_r}{\varepsilon_r\,+\,2}\,E \tag{6}$$

where ε_r is the relative permittivity of the dust particles. Substituting by (5) and (6) in (4) results in:

$$\rho_p = \frac{9\,\varepsilon_0\,EC_D}{gR_p}\,\frac{\varepsilon_r}{\varepsilon_r\,+\,2} \tag{7}$$

Indeed, the dust-loaded on the plate is non-uniformly distributed. In this work, we considered the non-uniform distribution of the dust particles. The space charge density of dust particles is a function of the number of dust particles per unit volume and the saturation charge acquired by the existing non-uniform electric field. In Eq. (7), the space charge density of dust particles at any node is a function of the calculated non-uniform field at this node.

After balancing electrical force with the Stokes drag force, the ion mobility of the dust particles can be calculated from:

$$K_p = \frac{\rho_p}{6\,\pi\,N_P\,\eta R_p} \tag{8}$$

where K_p represents the mobility of particles (m^2/V.s) and η is the viscosity of the gas.

2.3. Solution of poisson equation for dust loaded precipitators by FMG

The Poisson equation in the presence of dust particles is given by the following:

$$\nabla^2 V = -\,\frac{\rho\,+\,\rho_p}{\varepsilon_0} \tag{9}$$

where V, ρ, ρ_p, are ε_0 represent the applied potential variance, the ionic space charge density, the dust particle space charge density, and the free space permittivity, respectively. Further, the electric field is given by:

$$E = -\nabla V \tag{10}$$

Using the central finite difference method on Eq. (7):

$$\frac{\partial^2 V}{\partial x^2} \cong \frac{V_{i,j+1}\,+\,V_{i,j-1}\,-\,2\,V_{i,j}}{\Delta\,x^2} \tag{11}$$

$$\frac{\partial^2 V}{\partial y^2} \cong \frac{V_{i+1,j}\,+\,V_{i-1,1}\,-\,2\,V_{i,j}}{\Delta\,y^2} \tag{12}$$

Substituting by (11) and (12) in (9), the potential at any point in the computational grid is given by, as in Fig. 2:

$$V_{i,\,j} \cong (1-w)V_{i,\,j} + \frac{w}{2\,(\Delta\,x^2\,+\,\Delta\,y^2)}\left[\Delta\,x^2\left(V_{i+1,\;j}+V_{i-1,\;j}\right)+\;\Delta y^2\left(V_{i,\;j+1}+V_{i,\;j-1}\right)+\quad\frac{\Delta\,x^2.\,\Delta\,y^2}{\varepsilon_0}\left(\rho_{i,j}+\rho_{p_{i,\;j}}\right)\right] \tag{13}$$

Eq. (13) is solved iteratively by SOR, where; w is the relaxation factor, the SOR method becomes similar to the Gauss-Seidel iterative method.

The iterative solution of the Poisson equation is the key motive for requiring excessive time in the overall simulation to reach a particularly acceptable convergence. So, the Poisson equation will be solved iteratively using the FMG. Hence, FMG method works initially at the coarsest grid and solves it exactly by one of the traditional iterative methods and then the solution is interpolated to the finer grid where several V-cycles are completed. Fig. 3 illustrates the flowchart of one V–cycle. Here, it was demonstrated that N_1= 3 and N_2 = 1, give the best time performance in the issue.

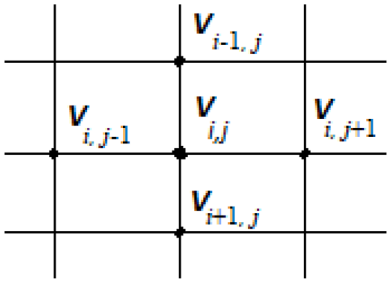

Fig. 2. Partial grid of fine computational domain.

2.4. Solution of continuity equation for dust loaded precipitators

The current continuity equation is given by:

$$\nabla \cdot J = 0 \tag{14}$$

in which J is the corona current density, the corona current density in presence of dust is given by:

$$J = \rho_p K_p E + \rho K E \tag{15}$$

in which K and K_p are the mobility of ions and dust particles, respectively, in m^2/V.s. Substituting by (15) in (14) results in,

$$\nabla \cdot E \left(\rho_p K_p + \rho K\right) + E \cdot \nabla \rho_p \cdot K_p + E \cdot \nabla \rho \cdot K = 0 \tag{16}$$

where the value of $\rho_p K_p$ is constant, so $\nabla \rho_p \cdot K_p = 0$. By applying backward finite-difference on (16) results in;

$$\rho_{i,j}{}^2 + A \rho_{i,j} + B = 0 \tag{17}$$

where,

$$A = \rho_p \left(1 + \frac{K_p}{K}\right) + \varepsilon_0 \left[\frac{E_x}{\Delta x} + \frac{E_y}{\Delta y}\right]$$

$$B = \rho_p{}^2 \frac{K_p}{K} - \varepsilon_0 \left[\rho_{i-1,j} \cdot \frac{E_x}{\Delta x} + \rho_{i,j-1} \cdot \frac{E_y}{\Delta y}\right]$$

in which E_x and E_y denote, respectively, the electric field intensities along with the x and y directions. The Δx and Δy values are symbolized the incremental spacing along with x-direction and y-direction, respectively. Through solving (12), the charge density value at any point, $\rho_{i,j}$ in the computational grid can be calculated, where;

$[I_{2h}^{h}]$: is the standard full weighting operator.

$[I_{h}^{2h}]$: is the bilinear interpolation operator.

2.5. Computational algorithm

The computational algorithm of FDM-FMG in dust loaded precipitators can be summarized as follows:

- Adjust the applied potential at the ionized wire, desired average current density, and apply all the boundary conditions into the system of equations.
- Compute the charge density at the surface of the wire using Eq. (1) and assume a primary guess for charge densities at every grid point.
- Solve Poisson equation at every grid point using Eq. (13) by FDM-FMG till a preset convergence is achieved.
- Recalculate the charge density at every point in the grid using Eq. (17) using the new values of potential calculated in the previous step.
- Check if the difference between each value of the potential at every point and its previous value is smaller than a prescribed error, if no go to step II.

The computational algorithm is terminated when the computed average current density at the plate understudy equals the wanted value, if not return to step I.

Regarding the dust layer, the charge density of dust particles is already included in the continuity equations which is solved by the finite difference method, as discussed in subSection 2.2. Where the ion mobility and the charge density of the dust particles are included in the continuity equation and the numerical procedures are as follows:

1) At every node in the computational domain, the charge density of the dust particles is calculated from Eq. (7). Hence, the charge density is a function of the electric field which is calculated by the proposed numerical technique FDM-FMG.

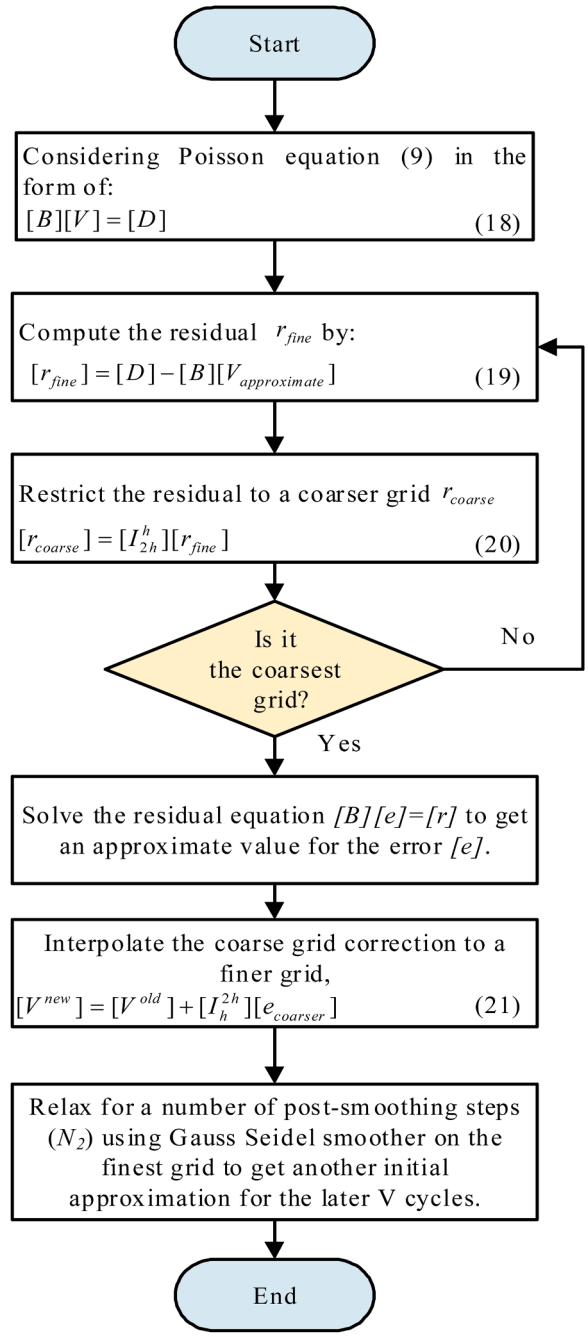

Fig. 3. flowchart of one V-cycle.

2) At every node in the computational domain, the ion mobility of the dust particles is calculated from Eq. (8).
3) Substituting by the values of particle charge density and the ion mobility of the dust particles from the previous points (1) and (2) in the continuity equation where it is solved at every node by the FDM.
4) Using the obtained values of the ion and particles charge densities to solve the Poisson equation to obtain the potential values at every node using the proposed FDM-FMG.

3. Results and discussion

3.1. The performance of FMG method on fine computational domains

As is well known, the Poisson equation is the most time-consuming portion of the corona issue modeling, particularly on fine grids. In the

current analysis, the Poisson equation is solved by FDM using the SOR technique and the FMG as iterative methods. An assessment between the SOR approach and the FMG method is carried out for Penny and Matick precipitator of wire diameter of 2.032 mm, the spacing between wires is equal 152.4 mm, and spacing between two grounded plates equals 228.6 mm [29]. The comparison is conducted for a grid size (129 × 129) points by means of Intel (R) Core (TM) i7–3612QM CPU @2.10 GHz.

The convergence characteristics of the voltage loop are assigned so that the percentage error is specified by Eq. (22) as follow;

$$error = \left|\frac{V_{new} - V_{old}}{V_{old}}\right| \times 100 \leq 10^{-6}\,\% \tag{22}$$

Fig. 4 displays the percentage potential error of SOR with a relaxation factor, $w = 1.8$, and the FMG method for 18 iterations. As seen in Fig. 4.a, the percentage error of the FMG method is 10% for the second iteration and drops by 92% for the fourth iteration, while in the case of SOR the percentage error at the second iteration is 6.4×10^5%, as in Fig. 4.b. FMG converges to the prescribed tolerance for a voltage loop after 18 iterations only while, in the case of SOR, it needs 20,380 iterations, so in terms of the speed-up factor, FMG decreases the effort by 1132. The overall program execution time for FMG is 1.8 s while for SOR is 230 s, so the computational time decreases by 99.22% on using FMG as an iterative solver on the grid (129 × 129). For the above observations, FMG converges faster than SOR, which in turn decreases the overall computational time.

The speedup factor is given by [2];

$$\text{speedup factor} = \frac{\text{number of iterations by Guass} - \text{Seidel}}{\text{number of iterations by FMG}} \tag{23}$$

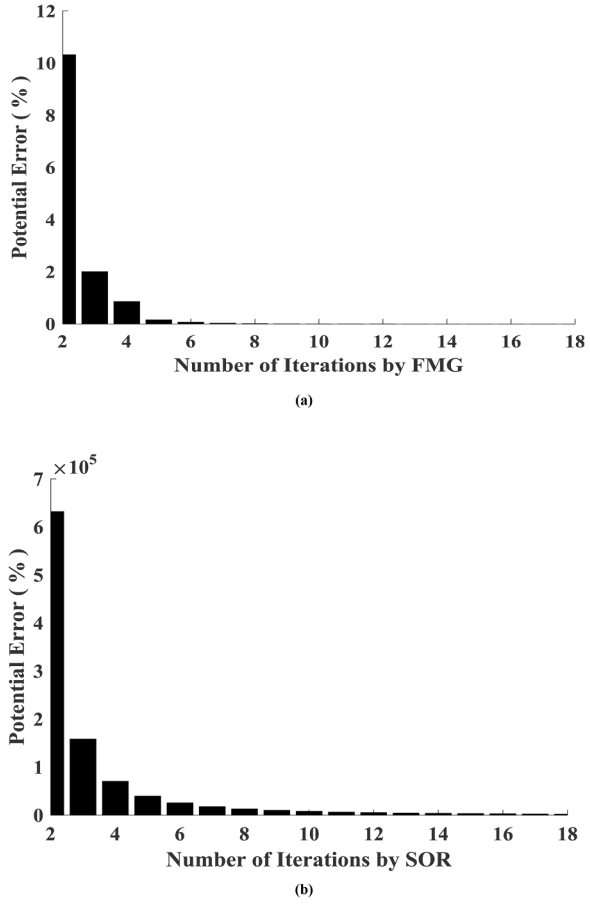

Fig. 4. Potential error vs. number of iterations by; (a) Full Multi-grid Method (FMG), and (b) Successive over relaxation (SOR).

Table I
The performance of FMG and SOR at different tolerances.

Desired tolerance	Number of iterations for voltage loop		Voltage loop execution time (s)		Overall program execution time (s)	
Grid of (129 × 129)	SOR w = 1.8	FMG	SOR w = 1.8	FMG	SOR w = 1.8	FMG
0.1%	7743	11	9	0.13	65	0.7
10^{-5}%	24,211	15	18	0.188	170	1.45
10^{-6}%	20,380	18	24	0.2	230	1.8

3.2. Performance of FMG on fine computational domains for different tolerances

Indeed, the tolerance to reach a certain convergence affects the performance of the iterative methods in terms of timing and the number of iterations required. As the desired tolerance decreases, more computational time and a greater number of iterations are required. The proposed method is used to study the performance of FMG and SOR for different tolerance values, which are presented in Table I. As shown in Table I, although the desired tolerance is 0.1%, FMG reduces the effort by a factor of 704 to terminate from the voltage loop only. Also, the time decreases by 99% as compared to SOR.

Besides, the present work performs a study to show if the tolerance affected the agreement between the numerical results and experimental values or not, as in Table II. The study is performed on Penny and Matick geometry for an applied voltage of 43.5 kV [29]. The results show that as tolerance decreases, the accuracy increases, but it does not dramatically change the results in this case and all these errors are acceptable, in the proposed technique.

Generally, as the tolerance decreases, the accuracy increases, and the computational time increases especially on finer grids. So, for a certain problem, FMG can be implemented for different tolerances without suffering from high computational time. This advantage is not found with the classical iterative techniques. So, by using FMG, researchers can work on small tolerances without facing the problem of computational time as compared to the SOR method.

3.3. Validation of FMG method for clean air precipitators

The proposed algorithm is conducted for Penny and Matick's geometry for ESP [29]. The ion mobility (k) is assumed to be 1.6×10^{-4} m^2/V.s, and the applied voltage is set to be 43.5 kV. The values of potential along BC and AD are computed and compared to the tested ones by Penny and Matick, as shown in Fig. 5.

3.4. Justification of the chosen ion mobility value for Penny and Matick geometry

For Penny and Matick geometry the ion mobilities used in previously published work are 1.82×10^{-4}, and 2.2×10^{-4} m^2/V.s [11, 12]. FDM-FMG implements these ion mobilities and investigates the numerical results. A detailed comparison between the numerical results and the experimental results are described in Table III.

For instance, in order to get a mean current density of 4.84×10^{-4} A/m^2 on the grounded plate understudy, a voltage of 42 kV is employed on the wire for actual ion mobility of 1.82×10^{-4} m^2/V.s. Further, this

Table II
The performance of the FMG at different tolerances.

Tolerance	V = 43.5 kV, $J_{exp} = 4.84 \times 10^{-4}$ A/m^2	
	J_{comp} ($\times 10^{-4}$)	Error (%)
0.1%	4.855	0.31
10^{-5}%	4.847	0.144
10^{-6}%	4.843	0.06

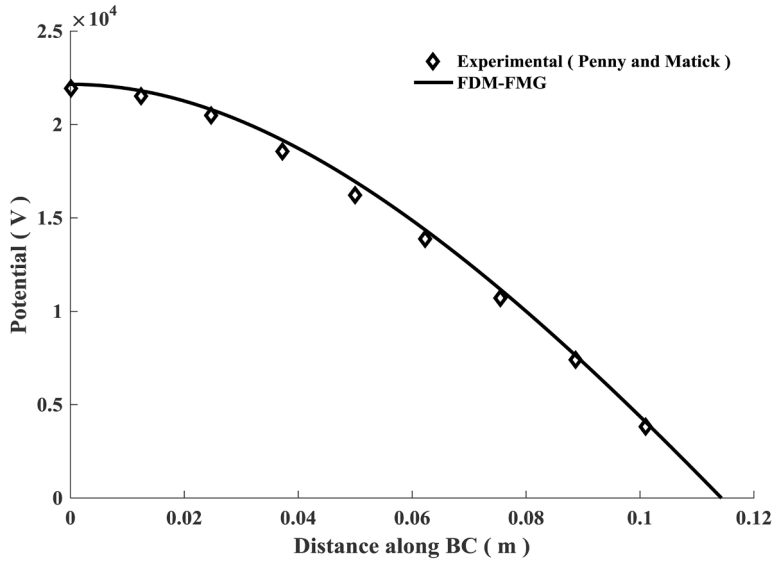

(a)

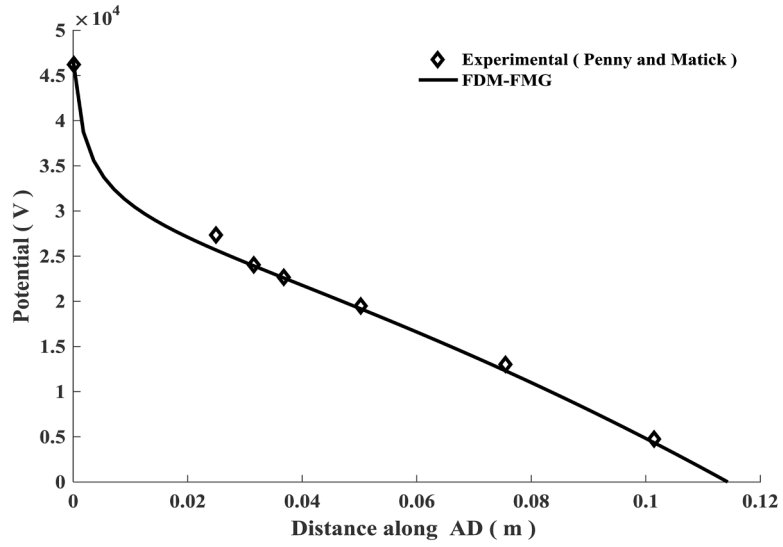

(b)

Fig. 5. The potential distribution along the distance; (a) BC, and (b) AD.

Table III
The performance of different ion mobilities on accuracy of numerical results.

Ion Mobility (m^2/Vs)	$V_{applied}$ = 43.5 kV, J_{exp} = 4.84 × 10^{-4} A/m^2		$V_{applied}$ = 46.2 kV, J_{exp} = 6.88 × 10^{-4} A/m^2	
	Numerically predicted voltage (kV)	Error (%)	Numerically predicted voltage (kV)	Error (%)
1.6×10^{-4}	43.5	0%	46.6	0.86%
1.82×10^{-4}	42	3.44%	45.2	2.16%
2.2×10^{-4}	41	5.7%	43.5	5.84%

value diverges from Penny's applied voltage by 3.44%. On using ion mobility of 2.2×10^{-4} m^2/V.s, a voltage of 41 kV is applied on the wire which diverges from Penny's applied voltage by 5.7%.

While employing ion mobility of 1.6×10^{-4} m^2/V.s results in a voltage of 43.5 kV, which is similar to Penny's applied voltage. Hence, ion mobility of 1.6×10^{-4} m^2/V.s becomes further confident rather than that of 1.82×10^{-4} m^2/V.s and 2.2×10^{-4} m^2/V.s involving Penny and Matick's experimental results. In addition, Elmoursi in his simulation predicts a wire voltage of 40.5 kV using a mobility value of 2.2×10^{-4} m^2/Vs relating to Penny and Matick's experimental results at a 43.5 kV value of applied voltage [12]. For more confirmation, the present algorithm gives the numerical and experimental results for different ion mobilities at applied voltages of 43.5 kV and 46.2 kV, as shown in Figs. 6 and 7, respectively. Again, the ion mobility of 1.6×10^{-4} m^2/V.s gives the best fit between the experimental values of Penny and numerical results at different voltages.

3.5. FMG method as a powerful prediction tool for V-I ch/s

The advantage of the fast convergence of the FMG as an iterative solver on fine computational domains can be used as a powerful prediction tool for the voltage-current characteristics instead of the costly

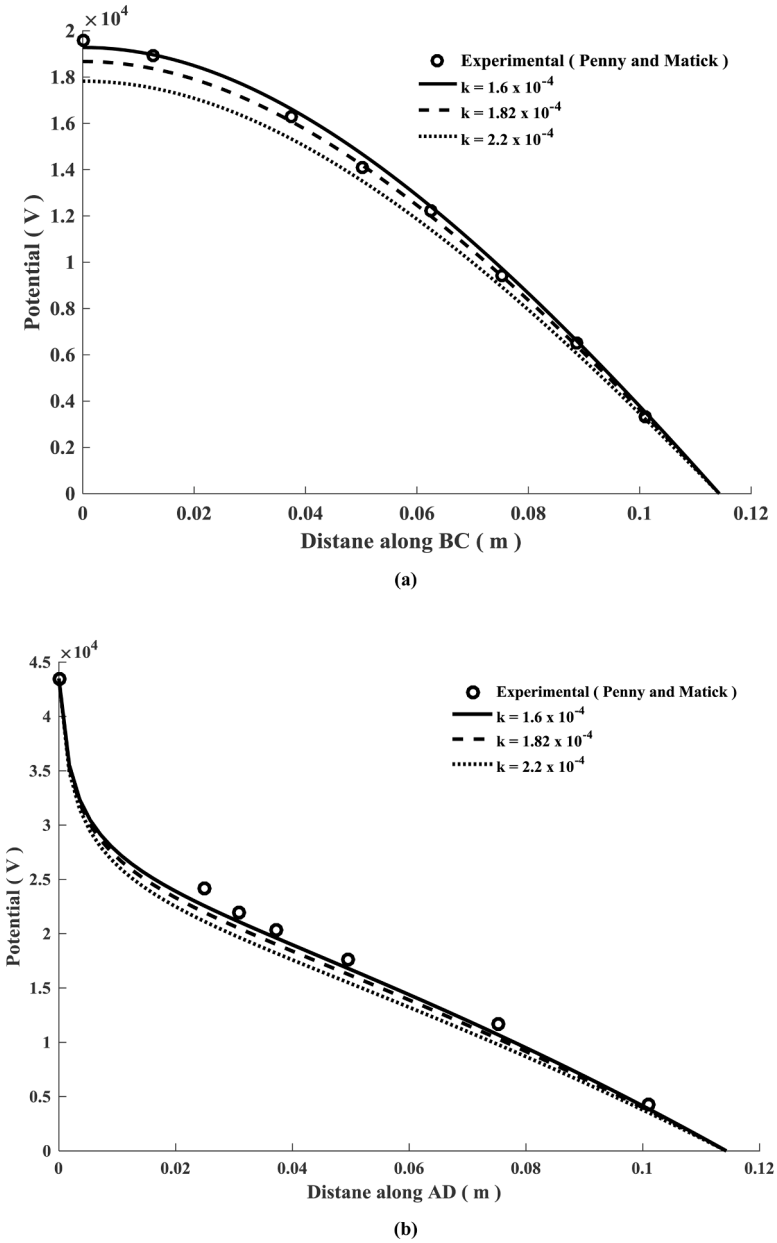

Fig. 6. The potential distribution at 43.5 kV with different values of ion mobility along the distance; (a) BC, and (b) AD.

experimental work. Accordingly, the present study performed a study on the Abdel-Salam model for precipitators [11], the geometry has a wire radius of 0.5 mm, the spacing between wires is 10 cm or 20 cm, and the spacing between plates is 13 cm or 18 cm or 23 cm. FDM-FMG is used to track the optimal grid size for this design of precipitators by using different sizes of grids up to (256 × 256) grid points.

Firstly, a study is conducted at different applied voltages as shown in Table IV, to track the optimal grid and it is pointed out that the optimal grid is (64 × 64). But there is a question here, does this grid is the optimal one if the wire height is changed, or if the wire to wire spacing is changed? To answer this question, a comparison is established and presented in Table V at an applied voltage of 28.1 kV, and it is found that the (64 × 64) is the optimal grid for different wire heights. Also, a study is conducted for the different wire to wire spacing, as in Table VI, and it is found that the (64 × 64) is the optimal grid. Although (128 × 128) grid can be optimal grid at $S_x = 5$ cm and $S_y = 9$ cm, but it can be considered as the local grid for these design parameters, but the grid (64 × 64) is the global optimal for this precipitator design.

So, the results confirm that using FMG as an iterative solver can be a powerful tool for the designers to predict the voltage-current characteristics at different design parameters without the need for costly experimental work.

3.6. Performance of FMG on fine computational domains in dust loaded precipitators

The proposed algorithm is used to model the dust-loaded precipitators. To test the effectiveness of the computational algorithm, the simulation is performed for cement dust particles having a dominant particle radius of 30 μm. The concentration of the dust particles is 18 gm/m^3 with a specific gravity of 1.69 gm/cm^3. The precipitator has a wire radius of 0.521 mm, plate-to-plate spacing equals 203.2 mm, and wire-to-wire spacing equals 203.2 mm [30]. The simulation is conducted on a fine computational domain of (256 × 256) grid points. The percentage potential error is shown in Fig. 8, FMG takes only 25 iterations to terminate from the voltage loop within 0.8 s. The overall execution

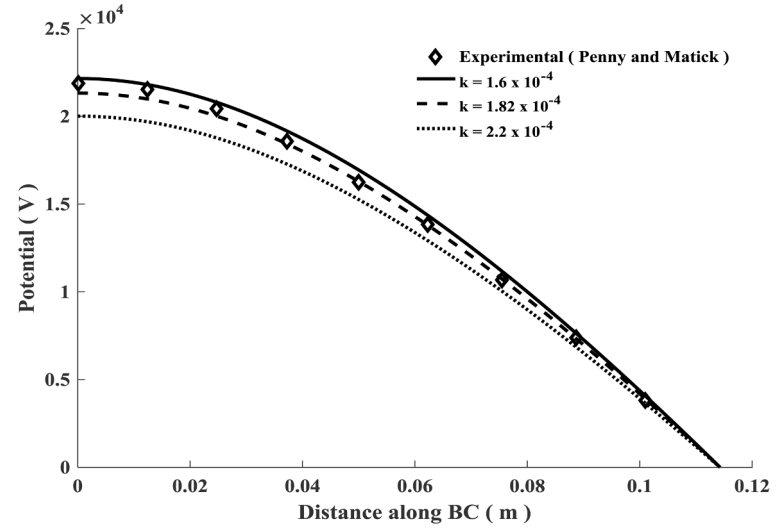

(a)

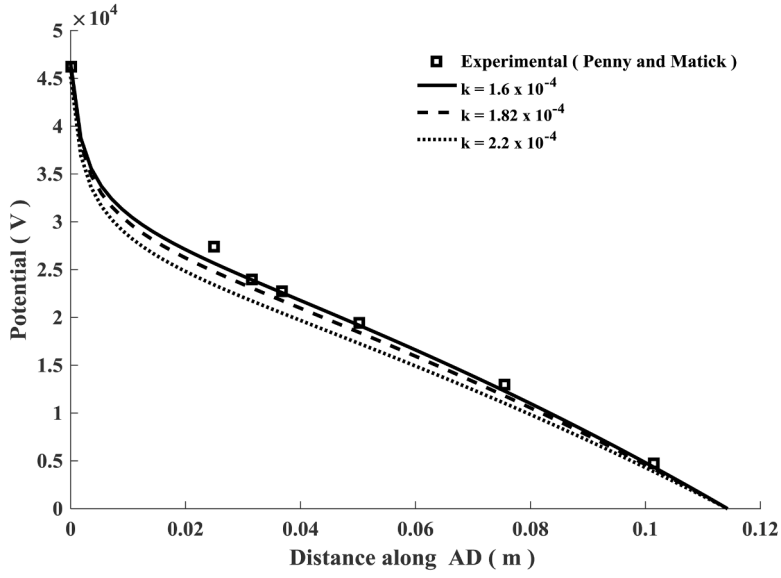

(b)

Fig. 7. The potential distribution at 46.2 kV with different values of ion mobility along the distance; (a) BC, and (b) AD.

Table IV
The performance of different grid sizes for different applied voltages.

S_x =5 cm, S_y =11.5 cm	V_{exp} = 28.1 kV, I_{exp} = 97 × 10^{-6} A/m		V_{exp} = 31 kV, I_{exp} = 154 × 10^{-6} A/m		V_{exp} = 33 kV, I_{exp} = 230 × 10^{-6} A/m	
Grid Size	Numerically predicted voltage (kV)	Error (%)	Numerically predicted voltage (kV)	Error (%)	Numerically predicted voltage (kV)	Error (%)
(16 × 16)	24.5	12.8	26	16	27	18
(32 × 32)	27	3.9	28	9.6	29	12
(64 × 64)	28.3	0.7	30.5	1.6	32.5	1.5
(128 × 128)	31	10.3	32.5	4.8	33.8	2.4
(256 × 256)	33.5	19	34.6	11.6	36	9

time for the whole program is 6 s.

In order to choose the optimal computational grid for this dust-loaded precipitator, the FDM-FMG method is conducted on fine computational domains up to (256 × 256) grid points, as in Fig. 9. The simulation results for the different grid sizes are compared to previous experimental results [30], and the following conclusions are noticed:

- The best grid size at an applied voltage of 23 kV is (33 × 33);
- The best grid size at an applied voltage of 27 kV is (65 × 65);
- The best grid size at applied voltages of 30.5 kV, 38 kV, 41 kV, 45 kV, and 49 kV are (256 × 256);
- For grid (513 × 513), as the grid becomes finer the error increases, this may be attributed to the increasing round-off error.

So, the global optimal grid for this design of the dust loaded precipitator that grantees both low truncation and roundoff error are (256

Table V
The performance of different grid sizes for different wire heights.

$V_{exp} = 28.1$ kV $S_x = 5$ cm Grid Size	$S_y = 6.5$ cm, $I_{exp} = 560 \times 10^{-6}$ A/m Numerically predicted voltage (kV)	Error (%)	$S_y = 9$ cm, $I_{exp} = 200 \times 10^{-6}$ A/m Numerically predicted voltage (kV)	Error (%)	$S_y = 11.5$ cm, $I_{exp} = 97 \times 10^{-6}$ A/m Numerically predicted voltage (kV)	Error (%)
(16 × 16)	23.2	17	22.2	21	24.5	12.8
(32 × 32)	24.8	11.7	24	14.6	27	3.9
(64 × 64)	27.8	1	27.2	3.2	28.3	0.7
(128 × 128)	29.5	4.9	29	3.2	31	10.3
(256 × 256)	32	13.8	31.2	11	33.5	19

Table VI
The performance of different grid sizes for different wire to wire spacing.

$V_{exp} = 28.1$ kV $S_y = 9$ cm	$S_x = 5$ cm, $I_{exp} = 200 \times 10^{-6}$ A/m		$S_x = 10$ cm, $I_{exp} = 286 \times 10^{-6}$ A/m	
Grid Size	Numerically predicted voltage (kV)	Error (%)	Numerically predicted voltage (kV)	Error (%)
(16 × 16)	22.2	21	22.2	21
(32 × 32)	24	14.6	27	3.9
(64 × 64)	27.2	3.2	29.1	3.5
(128 × 128)	29	3.2	32	13.8
(256 × 256)	31.2	11	34.5	22.7

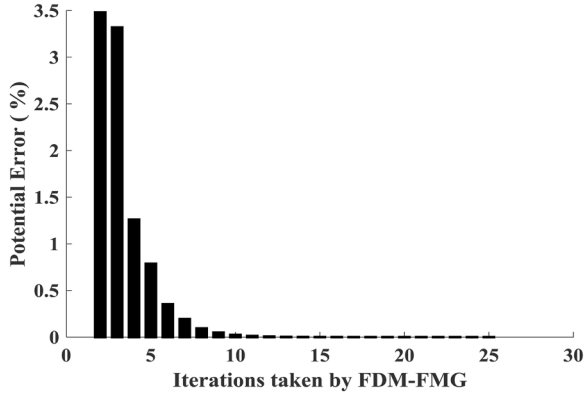

Fig. 8. Potential error vs. number of iterations by FDM-FMG.

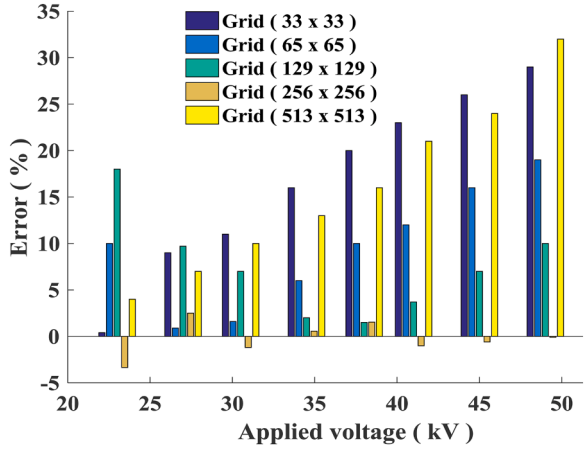

Fig. 9. Percentage error of different grid sizes.

× 256) with maximum percentage error from experimental results 3%, while grids (33 × 33) and (65 × 65) can be considered as local optimal grids at 23 kV and 27 kV only. The simulated voltage-current characteristics for the chosen global optimal grid (256 × 256) are compared with the experimental results [30], and an excellent agreement is reached as shown in Fig. 10.

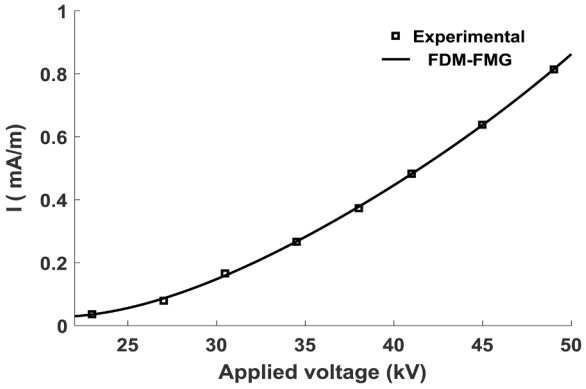

Fig. 10. Comparison between FDM-FMG and experimental V–I characteristics.

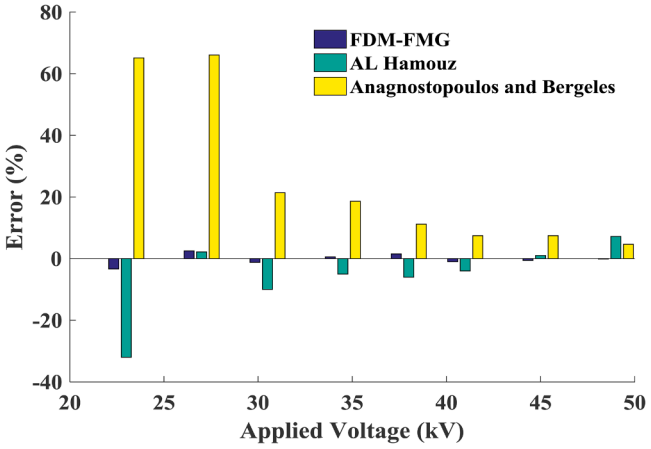

Fig. 11. Percentage error compared to experimental values. (For interpretation of the references to colour in this figure legend, the reader is referred to the web version of this article.)

Furthermore, for the same geometry, the present algorithm is tested against the FEM proposed by Al Hamoz et al. [19] and the method introduced by Anagnostopoulos et al. [31]. Fig. 11 shows the percentage of error between the three methods and the experimental values of the current. Generally, the percentage error from the experimental values is dramatically reduced at different applied voltages using FDM-FMG on a fine computational domain of (256 × 256) grid points without suffering from excessive computational time. Accordingly, the proposed method is an efficient predictive tool in the design stage of commercial precipitators.

3.7. FDM-FMG as a prediction tool for the effect of changing different design parameters on the current, ion, and particle charge densities

3.7.1. Effect of the variation of applied voltage on current density, and ion & particle densities

After choosing the optimal grid of (256 × 256) grid points for the

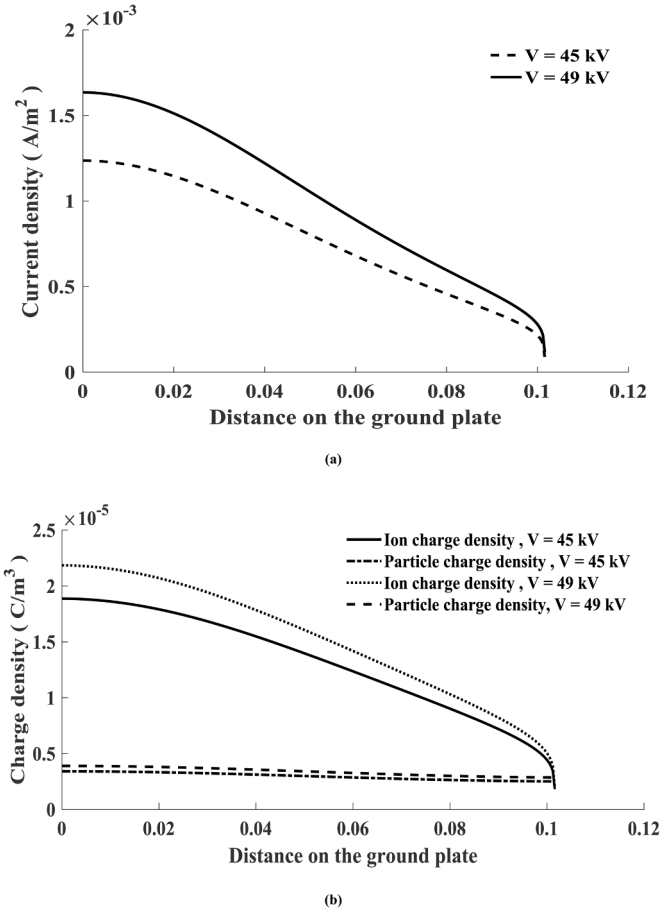

Fig. 12. Effect of the variation of applied voltage on; (a) current density, and (b) ion and particle charge densities.

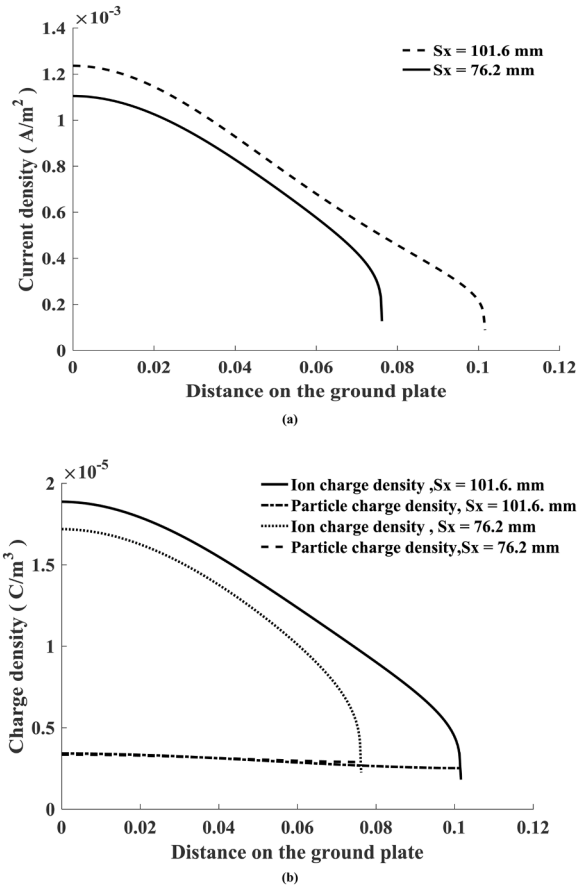

Fig. 13. Effect of the variation of wire to wire spacing on; (a) current density, and (b) ion and particle charge densities.

above-mentioned dusted loaded precipitator, FDM-FMG is implemented to predict the effect of changing the applied voltage on the current density as well as the ion and particle charge densities on the ground plate. The average current density increases by 32% when applied voltage increases from 45 kV to 49 kV, Fig. 12.a. Also, the average ion and particle densities increase by 15% and 13% when applied voltage increases from 45 kV to 49 kV, respectively, as in Fig. 12.b.

3.7.2. Effect of the variation of wire to wire spacing on current density, and ion & particle densities

Moreover, the effect of changing the wire-wire spacing on the current density as well as the ion and particle charge densities is conducted using FDM-FMG at an applied voltage of 45 kV. The average current and ion densities and decrease by 3% and 3.4% when S_x decreases from 101.6 mm to 76.2 mm respectively, as in Fig. 13. Also, the average particle density increases by 2% when S_x decreases from 101.6 mm to 76.2 mm, as in Fig. 13.b. This can be explained by the fact that as the spacing between wires decreases, the corona onset voltage increases as the number of the field lines on the wire decreases, resulting in a less corona current and hence a lower current density at the same applied voltage. It can be pointed out that change in the spacing between wires doesn't dramatically change the average current, ion, and particle densities on the grounded plate.

3.7.3. Effect of the variation of wire height on current density, and ion & particle densities

In addition, the effect of changing wire height above the ground plate on the average current and ion densities at an applied voltage of 45 kV is studied. The average current density increases by 123% when Sy decreases from 101.6 mm to 76.2 mm respectively, Fig. 14.a. Also, the average ion and particle densities increase by 43% and 18% when S_y decreases from 101.6 mm to 76.2 mm, respectively, as shown in Fig. 14. b. This can be attributed to the fact that as the height of ionized wire decreases, the corona onset voltage decreases, resulting in a higher corona current and hence a higher current density at the same applied voltage.

It can be pointed out that change in the height of the wire above the ground dramatically changes the average current, ion, and particle densities on the grounded plate, these densities are also affected by the change of the applied voltages on the ionizing wire. On the other side, the change in the spacing between wires did not have a significant effect on the current, ion, and particle densities. Fortunately, from the industrial point of view, if a desired high current density is needed for the charging process in dust-loaded precipitators, one can decrease the height or increase the applied voltage rather than increasing the distance between the ionized wires due to the limited size of the precipitators.

3.7.4. Discussions

Here, we provide the limitations of the current study for the modeling of ESPs. For the current problem in precipitators, the region is bounded, and the radius of the wire is small enough to consider it a single node in the computational domain. In most commercial precipitators the radius of the ionized wire is small with respect to the overall size of the precipitator. So, the finite difference method works well with such a problem. On the other hand, if the radius of the ionized wire is large, or the region is unbounded, the finite difference will be more difficult to implement as in the case of HVDC transmission lines [32, 33, 34]. it is better to formulate that problem with the finite

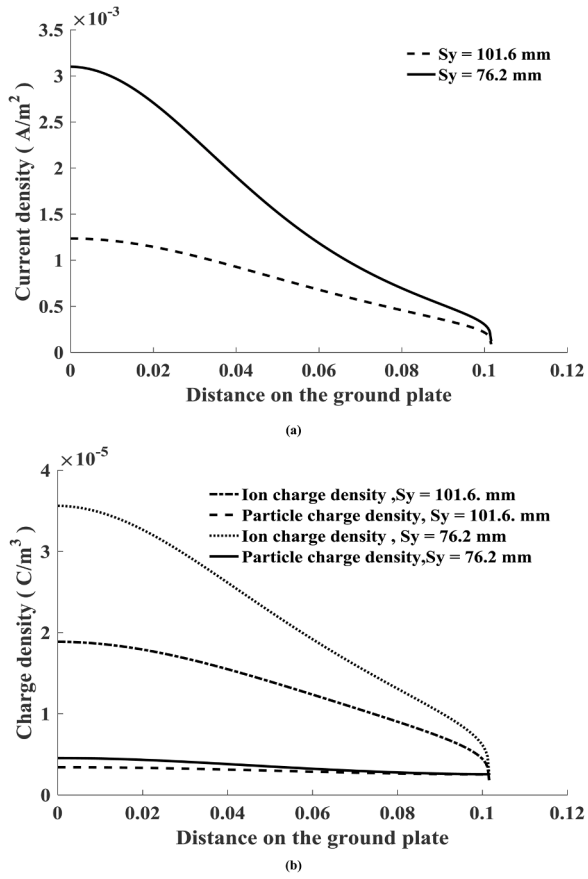

Fig. 14. Effect of the variation of wire height on; (a) current density, and (b) ion and particle charge densities.

element method, not the finite difference method. In a future study, we aim to integrate the finite element method with the multigrid methods and test its performance.

4. Conclusions

The paper presents a novel approach for modeling the dust-loaded electrostatic precipitators on the fine computational domain. For clean and dust-loaded precipitators, FMG is greatly transcendent over SOR in terms of convergence rate and hence the timing performance, especially on fine computational domains. The shortcomings of the different numerical methods and their remedy by the proposed FDM-FMG method implemented for the simulation of ESPs are summarized as follows:

- All the mentioned numerical techniques cannot work on fine computational domains without suffering from excessive computational time. So, the need for an efficient iterative solver is a must. In this regard, the present study implements the full multigrid method as an iterative solver which guarantees both fine domains and less computational time.
- The results of the previous techniques cannot be considered to get an accurate picture of the precipitators in the design stage. By the proposed technique, we can predict results without the need for costly experiments.
- The FDM-FMG solves Poisson and continuity equations on one fine computational domain and that is unavailable in the previous numerical methods.
- Unlike the previous numerical techniques, the present proposed method works on different tolerances regarding the convergence rate without suffering from the high computational time.

Besides, two advantages are introduced by the proposed technique for the first time due to working on fine computational grids without suffering from the high computational time:

- FDM-FMG gives a more confident value of the chosen ion mobility without the need for excessive experimental efforts to measure it.
- Choosing the optimal computational grid for any commercial dust-loaded precipitators that grantees both low truncation and round-off errors and can be a prediction tool for the change of different design parameters on the electrical conditions of the precipitator, and this advantage reduces the effort for the precipitator's designers.

Finally, the FDM-FMG strategy predicts that the electrical conditions are greatly affected by changing the applied voltage and the height of the ionized wires in dust-loaded precipitators which in turn affects the collection efficiency of the dust particles. In future work, the FDM-FMG method can be implemented in the design of advanced ESP-based air cleaning systems, such as electrostatic enhanced air filter, hybrid electrostatic filtration system, and electrostatic enhanced pleated air filters.

CRediT authorship contribution statement

Ahmad M. Sayed: Conceptualization, Software, Validation, Writing – original draft. **Mohamed A. Abouelatta:** Data curation, Writing – review & editing. **Mohamed Badawi:** Investigation, Visualization. **Karar Mahmoud:** Writing – review & editing, Resources, Formal analysis. **Matti Lehtonen:** Supervision, Funding acquisition. **Mohamed M. F. Darwish:** Methodology, Resources, Investigation, Writing – original draft.

Declaration of Competing Interest

The authors declare that they have no known competing financial interests or personal relationships that could have appeared to influence the work reported in this paper.

Acknowledgement

This work was supported by the Department of Electrical Engineering and Automation, School of Electrical Engineering, Aalto University, Finland, and by the high voltage laboratory, Faculty of Engineering at Shoubra, Benha University, Egypt.

References

[1] I.V.Muralikrishna Tian, V. Manickam, Chapter fourteen—air pollution control technologies. Environmental Management, Elsevier, Amsterdam, The Netherlands, 2017, pp. 337–397.
[2] A.M. Omar, M.A. Abouelatta, Fast corona discharge solver for precipitators using multi-grid methods on fine grids, IET Sci., Measurement Technol. 13 (3) (2018) 453–460.
[3] C.D. Tsadilas, E. Evangelou, Coal fly ash utilization for boron management in soils, plants, and waters. Environmental Materials and Waste, Academic Press, 2016, pp. 647–663.
[4] J. Hammerschmidt, J. Güntner, B. Kerstiens, A. Charitos, Roasting of gold ore in the circulating fluidized-bed technology. Gold Ore Processing, Elsevier, 2016, pp. 393–409.
[5] K. Adamiak, Numerical models in simulating wire-plate electrostatic precipitators: a review, J. Electrostat. 71 (4) (2013) 673–680.
[6] Hong Lei, Lian-Ze Wang, Zi-Niu Wu, Applications of upwind and downwind schemes for calculating electrical conditions in a wire–plate electrostatic precipitator, J. Comput. Phys. 193 (2) (2004) 697–707.
[7] Jack R. McDonald, B. Wallace, Herbert W. Smith, I.I.I. Spencer, Leslie E. Sparks, A mathematical model for calculating electrical conditions in wire-duct electrostatic precipitation devices, J. Appl. Phys. 48 (6) (1977) 2231–2243.
[8] Gregory A. Kallio, David E. Stock, Computation of electrical conditions inside wire-duct electrostatic precipitators using a combined finite-element, finite-difference technique, J. Appl. Phys. 59 (6) (1986) 1799–1806.
[9] Kazimierz. Adamiak, Simulation of corona in wire-duct electrostatic precipitator by means of the boundary element method, IEEE Trans. Ind. Appl. 30 (2) (1994) 381–386.

[10] B.S. Rajanikanth, N. Thirumaran, Prediction of pre-breakdown V–I characteristics of an electrostatic precipitator using a combined boundary element-finite difference approach, Fuel Processing Technol. 76 (3) (2002) 159–186.
[11] M. Abdel-Salam, A. Eid, Finite element simulation of corona in wire-duct precipitators. Conference Record of the 2002 IEEE Industry Applications Conference. 37th IAS Annual Meeting (Cat. No. 02CH37344), vol. 2, IEEE, 2002, pp. 1383–1389.
[12] Alaa A. Elmoursi, G.S. Peter Castle, Modeling of corona characteristics in a wire-duct precipitator using the charge simulation technique, IEEE Trans. Ind. Appl. 1 (1987) 95–102.
[13] Zakariya Al-Hamouz, Amer El-Hamouz, Nabil Abuzaid, Simulation and experimental studies of corona power loss in a dust loaded wire-duct electrostatic precipitator, Adv. Powder Technol. 22 (6) (2011) 706–714.
[14] Zakariya Mahmoud Al-Hamouz, A combined algorithm based on finite elements and a modified method of characteristics for the analysis of the corona in wire-duct electrostatic precipitators, IEEE Trans. Ind. Appl. 38 (1) (2002) 43–49.
[15] James L. Davis, James F. Hoburg, Wire-duct precipitator field and charge computation using finite element and characteristics methods, J. Electrostat. 14 (2) (1983) 187–199.
[16] S. Cristina, M. Feliziani, Calculation of ionized fields in DC electrostatic precipitators in the presence of dust and electric wind, IEEE Trans. Ind. Appl. 31 (1995) 1446–1451.
[17] W.S. Bracha, G.S.P. Castle, Electrical conditions in dust loaded wire-duct precipitators, IEEE Ind. Appl. Society Ann. Meeting 2 (1988) 1652–1656.
[18] S. Abdel-Sattar, A.A. Ibrahim, On the wire-duct electrostatic precipitator. IEEE Industrial Applications Soc., Annual. Meeting Denver, CO, 1986, pp. 1113–1118.
[19] Zakariya Al-Hamouz, Amer El-Hamouz, Analysis of a wire–duct electrostatic precipitator under dust loading conditions, Energy conversion Manag. 52 (2) (2011) 1235–1243.
[20] Maria Jedrusik, Arkadiusz Swierczok, Ryszard Teisseyre, Experimental study of fly ash precipitation in a model electrostatic precipitator with discharge electrodes of different design, Powder Technol. 135 (2003) 295–301.
[21] J. Miller, B. Hoferer, A.J. Schwab, The impact of corona electrode configuration on electrostatic precipitator performance, J. Electrostat. 44 (1–2) (1998) 67–75.
[22] Ye Zhuang, Yong Jin Kim, Tai Gyu Lee, Pratim Biswas, Experimental and theoretical studies of ultra-fine particle behavior in electrostatic precipitators, J. Electrostat. 48 (3–4) (2000) 245–260.
[23] G. Bacchiega, I. Gallimberti, E. Sani, R. Sala, V. Arrondel, M. Hamlil, E. Christensen, Experimental study of the mass balance in a pilot industrial electrostatic precipitator, J Electrostat 64 (5) (2006) 297–309.
[24] Mohamed A. Abouelatta, A.M. Omar, Sayed Ward, Optimal grid size for precipitators using finite difference method based on full multi-grid method, Electric Power Syst. Res. 189 (2020), 106575.
[25] M.A. Abouelatta, S.A. Ward, Ahmad M. Sayed, K. Mahmoud, M. Lehtonen, M.M. F. Darwish, Fast Corona Discharge Assessment Using FDM integrated With Full Multigrid Method in HVDC Transmission Lines Considering Wind Impact, IEEE Access 8 (2020) 225872–225883.
[26] Sayed A. Ward, Adel El-Faraskoury, Mohamed Badawi, Shimaa A. Ibrahim, Karar Mahmoud, Matti Lehtonen, Mohamed MF Darwish, Towards Precise Interpretation of Oil Transformers via Novel Combined Techniques Based on DGA and Partial Discharge Sensors, Sensors 21 (6) (2021) 2223.
[27] Sherif SM Ghoneim, Sobhy S. Dessouky, Ahmed Boubakeur, Adel A. Elfaraskoury, Ahmed B.Abou Sharaf, Karar Mahmoud, Matti Lehtonen, Mohamed MF Darwish, Accurate insulating oil breakdown voltage model associated with different barrier effects, Processes 9 (4) (2021) 657.
[28] Abdelrahman M. Alshehawy, Diaa-Eldin A. Mansour, M. Ghali, Matti Lehtonen, Mohamed MF Darwish, Photoluminescence Spectroscopy Measurements for Effective Condition Assessment of Transformer Insulating Oil, Processes 9 (5) (2021) 732.
[29] Gaylord W. Penney, Richard E. Matick, Potentials in DC corona fields, Trans. Am. Institute of Electrical Eng., Part I: Commun. Electronics 79 (2) (1960) 91–99.
[30] Noel J. Felici, Recent advances in the analysis of the dc ionized fields-part II, Direct Current 8 (1963) 278–287.
[31] J. Anagnostopoulos, G. Bergeles, Corona discharge simulation in wire-duct electrostatic precipitator, J. Electrostat 54 (2) (2002) 129–147.
[32] Mohamed A. Abouelatta, Sayed A. Ward, Ahmad M. Sayed, Karar Mahmoud, Matti Lehtonen, Mohamed MF Darwish, Measurement and assessment of corona current density for HVDC bundle conductors by FDM integrated with full multigrid technique, Electric Power Syst. Res. 199 (2021), 107370.
[33] M. Elsisi, M.-.Q. Tran, K. Mahmoud, D.A. Mansour, Matti Lehtonen, Mohamed M. F. Darwish, Towards secured online monitoring for digitalized gis against cyber-attacks based on iot and machine learning, IEEE Access 9 (2021) 78415–78427.
[34] Sherif SM Ghoneim, Karar Mahmoud, Matti Lehtonen, Mohamed MF Darwish, Enhancing diagnostic accuracy of transformer faults using teaching-learning-based optimization, IEEE Access 9 (2021) 30817–30832.